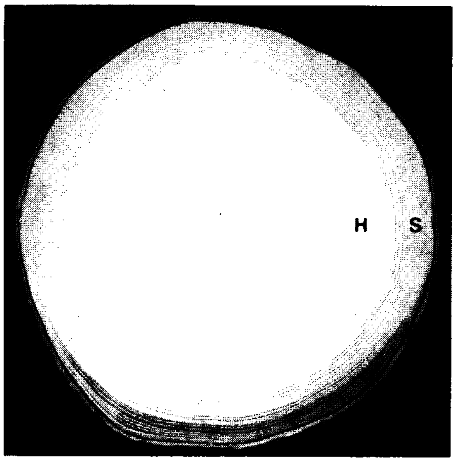

Fig. 2. Red spruce stem in transverse section. The sapwood (S) is visually distinguishable from the heartwood core (H) because the cut surface was sanded immediately after sectioning and photographed before the surface was allowed to dry. After drying, the distinction between S and H is not apparent.

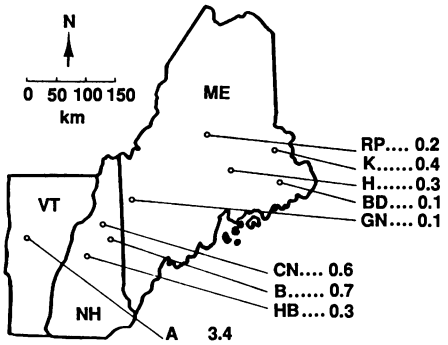

Fig. 3. Map of the red spruce study plots; A, Mount Abraham; CN, Crawford Notch; B, Bartlett; HB, Hubbard Brook; RP, Roach Pond; K, Kossuth; H, Howland; BD, Beddington; GN, Grafton Notch. Listed with the plots are the molar ratio values of Al:Ca in fine roots collected from the humus layer. The mean ratio for Mount Abraham was significantly different from that of all other locations ($P < 0.05$). Methods of analysis are given in (*2, 3*).

is a logical consequence of the progressive loss of sapwood basal area. The increased Ca demand of old trees and diminishing Ca supply may have hastened their decline; young trees are also declining in several areas (*1*). Once a tree has less than 25% sapwood in its cross-sectional area, it becomes highly vulnerable to death from secondary pathogens and insects (*11*). Trees at high elevation sites have apparently been most affected because the molar Al to Ca ratio is greater than one in both the humus (which contains the majority of absorbing fine roots) and the mineral subsoil (*3*).

Whether input of acids that are derived from sulfur and nitrogen emissions has caused the low soil *p*H conditions extant across the spruce-fir forests in the northeastern United States and Germany is moot. Continued input of strong anions of sulfur and nitrogen will increase amounts of Al in solution. This increase in Al concentration will reduce uptake of Ca through competition for binding sites in the cortical apoplast of fine roots. The problem is not one of Al toxicity (that is, an irreversible effect on the symplast), although this can happen with prolonged exposure to high Al concentrations, but rather a simple exchange phenomenon that can limit the rate of wood formation, decrease the amount of functional sapwood, and leave large trees more vulnerable to common diseases and insect pests. Similarly, any additional abiotic stress such as chronic air or soil pollution levels will also accelerate decline in trees that have already been weakened by the Ca deficiency syndrome.

REFERENCES AND NOTES

1. J. W. Hornbeck and R. B. Smith, *Can. J. For. Res.* **15**, 1199 (1985); P. Schutt and E. B. Cowling, *Plant Dis.* **69**, 548 (1985).
2. B. Ulrich, in *Effects of Air Pollution on Forest Ecosystems*, B. Ulrich and J. Pankrath, Eds. (Reidel, Dordrecht, 1983), pp. 1–32; J. Bauch, *ibid.*, pp. 377–386; H. Stienen, thesis, University of Hamburg (1985).
3. W. C. Shortle and H. Stienen, in *The Effects of Atmospheric Pollution on Spruce and Fir Forests in the Eastern United States and the Federal Republic of Germany* (U.S. Department of Agriculture, General Technical Report, Forest Service, Northeastern Forest Experiment Station, Broomall, PA, in press).
4. D. T. Clarkson and J. Sandersen, *J. Exp. Bot.* **22**, 837 (1971); J. Bauch, in *SO_2 und die Folgen* (Gesellschaft für Strahlen- und Umweltforschung GmbH-Bericht, Munchen-Neuherberg, 1983), pp. 49–57.
5. Newly formed red spruce sapwood contains 6.44 ± 0.71 μmol of Ca per cubic centimeter ($P < 0.05$) (*6*).
6. Calcium concentrations of spruce wood were determined by atomic absorption spectroscopy (*7*) and expressed as micromoles of dry tissue per cubic centimeter. No significant differences in molar Ca were evident for outer sapwood that formed 1.4 m above ground among locations. There was a small, but significant, increase in molar Ca concentration as sapwood was transformed into the dry heartwood core. Differences in mean values were determined by analysis of variance and tested at the $P = 0.05$ level of significance.
7. L. O. Safford, A. L. Shigo, M. Ashley, *Can. J. For. Res.* **4**, 435 (1974).
8. R. K. Bamber and K. Fukazawa, *For. Abstr.* **46**, 567 (1985).
9. J. Bauch, *Int. Assoc. Wood Anatomists Bull.* (new series) 7, 269 (1986); A. L. Shigo and W. E. Hillis, *Ann. Rev. Phytopathol.* **11**, 197 (1973).
10. Relation of red spruce foliage mass (y_1) and leaf area (y_2) to sapwood conducting area (x) from P. J. Marchand [*Can. J. For. Res.* **14**, 85 (1984)]:

$$y_1 = 0.072x - 0.410 \quad (r^2 = 0.84)$$
$$y_2 = 0.167x + 6.772 \quad (r^2 = 0.87)$$

11. W. C. Shortle and J. Bauch, *Int. Assoc. Wood Anatomists Bull.* (new series) 7, 375 (1986).
12. H. Stienen, R. Barckhausen, H. Schaub, J. Bauch, *Forstwiss. Centralbl.* **103**, 262 (1984).
13. G. E. Taylor, Jr., *et al.*, *Oecologia* **70**, 163 (1986).
14. C. S. Cronan and C. L. Schofield, *Science* **204**, 304 (1979).
15. W. Berneike *et al.*, in *Fortschritte in der atomspectromischen Spurenanalytik, Bd 2* (VCH Verlagsgesellschaft mbH, Weinheim, Federal Republic of Germany, 1986), pp. 505–515; P. Rademacher, J. Bauch, J. Puls, *Holzforschung* **40**, 331 (1986).
16. C. A. Federer and J. W. Hornbeck, *Can. J. For. Res.* **17**, 266 (1987).
17. A. L. Shigo, *Sci. Am.* **252**, 96 (April 1985); *J. For.* **83**, 668 (1985).
18. We are grateful for the technical expertise of K. R. Dudzik, P. J. Krusic, and G. P. Sredzienski.

16 December 1987; accepted 22 March 1988

Antarctic Ozone Depletion Chemistry: Reactions of N_2O_5 with H_2O and HCl on Ice Surfaces

MARGARET A. TOLBERT, MICHEL J. ROSSI, DAVID M. GOLDEN

The reactions of dinitrogen pentoxide (N_2O_5) with H_2O and hydrochloric acid (HCl) were studied on ice surfaces in a Knudsen cell flow reactor. The N_2O_5 reacted on ice at 185 K to form condensed-phase nitric acid (HNO_3). This reaction may provide a sink for odd nitrogen (NO_x) during the polar winter, a requirement in nearly all models of Antarctic ozone depletion. A lower limit to the sticking coefficient, γ, for N_2O_5 on ice is 1×10^{-3}. Moreover, N_2O_5 reacted on HCl-ice surfaces at 185 K, with γ greater than 3×10^{-3}. This reaction, which produced gaseous nitryl chloride ($ClNO_2$) and condensed-phase HNO_3, proceeded until all of the HCl within the ice was depleted. The $ClNO_2$, which did not react or condense on ice at 185 K, can be readily photolyzed in the Antarctic spring to form atomic chlorine for catalytic ozone destruction cycles. The other photolysis product, gaseous nitrogen dioxide (NO_2), may be important in the partitioning of NO_x between gaseous and condensed phases in the Antarctic winter.

CHEMICAL THEORIES FOR ANTARCTIC ozone depletion generally rely on catalytic ozone destruction cycles promoted by active chlorine (Cl and ClO) in the stratosphere (*1–6*). Moreover, only low levels of NO_x can be present or else the active chlorine will be scavenged. Because

---

Department of Chemical Kinetics, Chemical Physics Laboratory, SRI International, Menlo Park, CA 94025.

purely homogeneous chemical reactions do not meet these requirements, heterogeneous reactions on the surfaces of polar stratospheric clouds (PSCs) are thought to play a central role in the dramatic decrease in ozone recently observed in the Antarctic spring (*1–5*).

Recent laboratory studies have shown that heterogeneous reactions can occur efficiently on surfaces that simulate PSCs. For example, reactions 1 and 2 of chlorine nitrate ($ClONO_2$)

$$ClONO_2 + H_2O \rightarrow HOCl(g) + HNO_3(s) \quad (1)$$

$$ClONO_2 + HCl \rightarrow Cl_2(g) + HNO_3(s) \quad (2)$$

have been observed on ice and HNO_3-ice surfaces at 185 K (*7–9*). These reactions convert stable chlorine reservoir species ($ClONO_2$, HCl) into photochemically active forms of chlorine (HOCl, Cl_2, Cl_2O). Furthermore, the HNO_3 formed in these reactions remained condensed in the ice, providing a sink for NO_x.

Other possible heterogeneous reactions of importance in the Antarctic stratosphere are the reactions of N_2O_5 on PSCs. For example, reactions 3 and 4

$$N_2O_5 + H_2O \rightarrow 2\ HNO_3(s) \quad (3)$$

$$N_2O_5 + HCl \rightarrow ClNO_2(g) + HNO_3(s) \quad (4)$$

would deplete NO_x through the formation of condensed-phase HNO_3. Reaction 4 converts the stable reservoir species HCl into $ClNO_2$, which can be photolyzed readily in the Antarctic spring (cross section $\sigma = 1.55 \times 10^{-19}$ cm^2 at 300 nm) to efficiently produce atomic chlorine for ozone depletion (*10*). Reaction 4 also affects the balance between gaseous and condensed-phase NO_x. The springtime photolysis of $ClNO_2$ from this reaction produces gaseous NO_2, therefore preventing total condensation of NO_x during the polar winter.

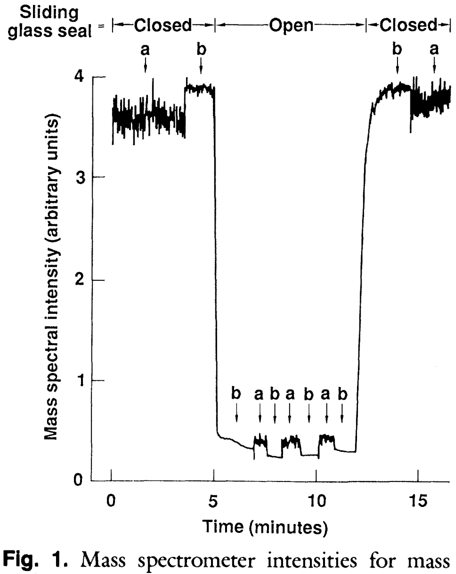

Fig. 1. Mass spectrometer intensities for mass peaks (**a**) *m/e* 30 (expanded ×2.5) and (**b**) *m/e* 46, for the reaction of N_2O_5 (P = 1.0 mtorr) on ice at 185 K. The N_2O_5 was exposed to ice only when the sliding glass seal was in the open position.

Neither reaction 3 nor reaction 4 has yet been reported to occur in the laboratory under Antarctic conditions (*11*). However, reaction 3 has been proposed as important in the Antarctic stratosphere (*3, 12*). In the ozone depletion model proposed by Crutzen *et al.* (*3*), reaction 3 is assumed to occur on the surfaces of PSCs during the polar night, resulting in low levels of NO_x. Their model indicates that in the absence of NO_2 and HNO_3, hydroxyl radicals (OH) react with HCl, liberating active chlorine for catalytic ozone destruction cycles. Recently, Wofsy *et al.* (*5*) suggested that reaction 4 may affect the NO_x-HCl balance in the Antarctic stratosphere. In their model, changes in the NO_x-HCl balance in the last 10 years are used to explain the abrupt onset of Antarctic ozone depletion in the late 1970s. We report that N_2O_5 reacts readily with both condensed H_2O and HCl at low temperatures on ice and HCl-ice surfaces.

We studied reactions 3 and 4 with a modified version of a Knudsen cell flow reactor (*8, 13*). We found that N_2O_5 reacted readily on ice to form condensed-phase HNO_3 (reaction 3). The steady-state intensities of the peaks with mass-to-charge ratios (*m/e*) of 46 and 30 were greatly reduced after exposure of N_2O_5 to ice at 185 K (*14*) (Fig. 1), revealing the loss of gas-phase N_2O_5.

The formation of condensed product, HNO_3, was detected in thermal desorption spectrometry (TDS) by its parent mass peak (*m/e* 63). Figure 2a displays the HNO_3 TDS signal after reaction of N_2O_5 (pressure P = 1.0 mtorr) on ice for 15 minutes at 185 K; Fig. 2b displays the impurity HNO_3 signal after exposure of N_2O_5 at the same pressure to halocarbon wax–coated copper for 15 minutes at 185 K. Much more HNO_3 was produced in the reaction of N_2O_5 on ice than was present as a result of impurities, indicating the occurrence of reaction 3.

Two HNO_3 desorption peaks (203 K and 230 K) were observed after the reaction of N_2O_5 with ice (Fig. 2a). The peak at 203 K is consistent with desorption of overlayers of "bulk" HNO_3. We believe that the peak at 230 K is due to the desorption of HNO_3 hydrates, such as $HNO_3 \cdot H_2O$ or $HNO_3 \cdot 3\ H_2O$ (*4*).

TDS scans of pure H_2O and of H_2O after reaction 3 are shown in Fig. 2, c and d. The desorption maximum for pure H_2O occurs at 209 K. Desorption of H_2O after reaction 3 shows two maxima, at 209 and 230 K. Thus, the desorption peaks at 230 K in Fig. 2, a and d, are probably due to bound HNO_3 and water, respectively, in the form of HNO_3 hydrates. TDS scans of HNO_3 after cocondensation of HNO_3 and H_2O indicated that the hydrate desorbs near 230 K.

The laboratory reaction of N_2O_5 on ice produced both tightly bound HNO_3 hydrates and overlayers of HNO_3. The HNO_3 overlayers may be due to the fairly high ratio of N_2O_5:H_2O used. Most of the total deposited water is used in the formation of HNO_3 hydrates, and there is little "free" water available for reaction (Fig. 2d). Overlayers of HNO_3 may be much less likely to form on the surfaces of PSCs because of the much lower concentrations of N_2O_5 in the stratosphere.

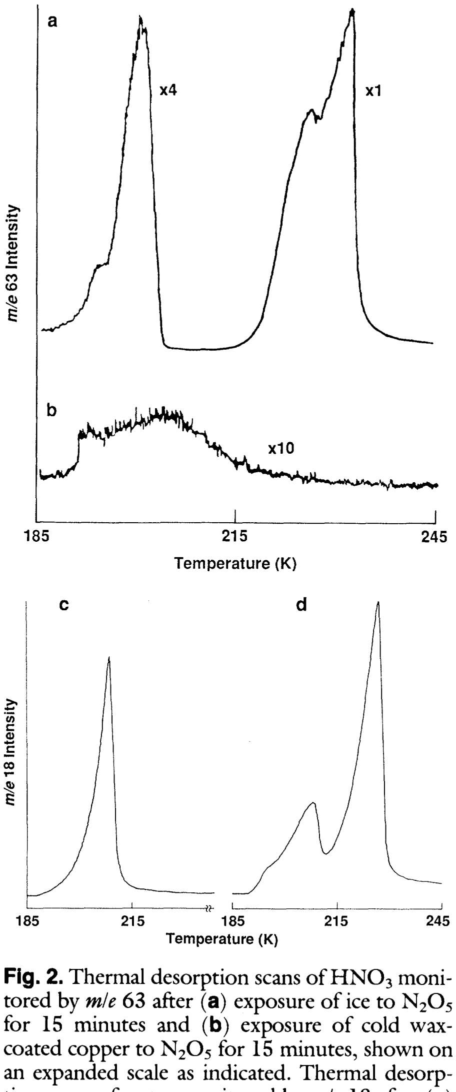

Fig. 2. Thermal desorption scans of HNO_3 monitored by *m/e* 63 after (**a**) exposure of ice to N_2O_5 for 15 minutes and (**b**) exposure of cold wax-coated copper to N_2O_5 for 15 minutes, shown on an expanded scale as indicated. Thermal desorption scans of water monitored by *m/e* 18 after (**c**) deposition of pure H_2O onto wax-coated copper at 185 K and (**d**) reaction of N_2O_5 on ice at 185 K.

The reaction efficiency for N_2O_5 on ice can be characterized by either the loss of gas-phase N_2O_5 or the formation of condensed-phase HNO_3. The relative collision efficiency for N_2O_5 loss on ice is given by the sticking coefficient, γ (*15*). Because N_2O_5 does not have a parent mass peak, γ was measured using mass peaks *m/e* 46 and 30 (Fig. 1). Unfortunately, the significant vapor pressure of HNO_3 at 185 K from the overlayers contributed to the mass spectrometer signals at these masses. A possible gas-phase reaction product, NO_2, also has mass peaks at *m/e* 46 and 30 that could cause interference. Thus, only a lower limit to the sticking coefficient for N_2O_5 on ice [$\gamma > 1 \times 10^{-3}$ ($\pm$50% in ten measurements)] could be determined.

We measured the efficiency of HNO_3 production by comparing the total amount of desorbed HNO_3 to the total amount of N_2O_5 exposed to the ice. A HNO_3:N_2O_5 ratio of 1.3 was determined for a 5-minute exposure of N_2O_5 to ice at 185 K. This ratio was based on the amount of N_2O_5 that entered the Knudsen cell. If all of the incoming N_2O_5 formed HNO_3 with unit efficiency, a ratio of 2.0 would be expected for reaction 3. The lower ratio observed suggests either that reaction 3 proceeds with less than unit efficiency or that other products, such as NO_2, are formed in the reaction. Unfortunately, unambiguous identification of NO_2 was not possible because its mass fragmentation peaks (*m/e* 30 and 46) were also observed for N_2O_5 and HNO_3.

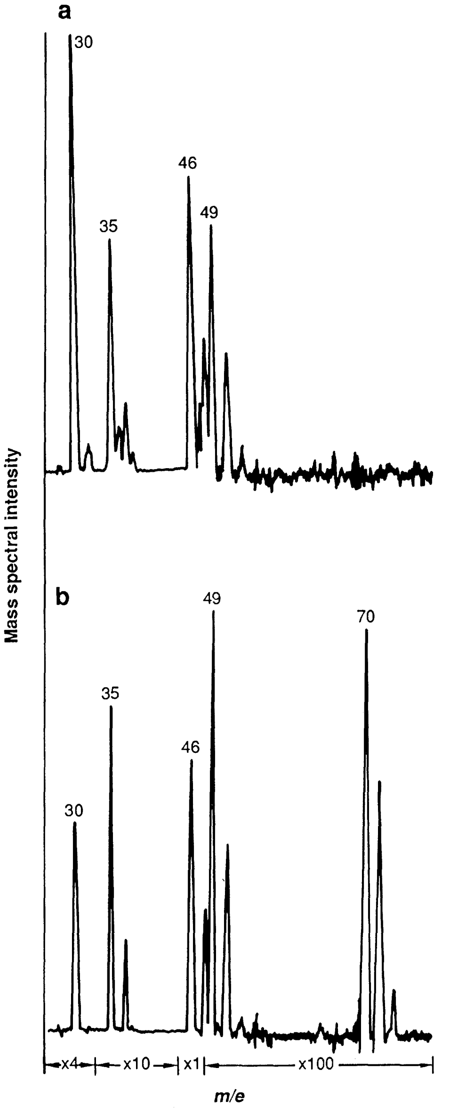

Fig. 3. Mass scans of the Knudsen cell effluent for (**a**) the reaction of N_2O_5 with HCl on wax-coated copper at 185 K and (**b**) gas-phase $ClNO_2$.

The reaction of N_2O_5 with HCl was studied on HCl-ice surfaces and on a cold halocarbon wax-coated copper surface. Reaction 4 proceeded readily in both cases at low temperature with formation of gas-phase $ClNO_2$ and condensed-phase HNO_3. Although N_2O_5 did not react with HCl on room-temperature wax-coated copper, there was a rapid reaction on cold wax-coated copper (185 K). The mass spectrum before reaction of N_2O_5 with HCl ($P_{N_2O_5} = 12$ mtorr, $P_{HCl} = 5$ mtorr) shows the characteristic N_2O_5 peaks (*14*) along with peaks due to HCl [*m/e* 35(37) from $^{35}Cl(^{37}Cl)$ and 36(38) with *m/e* 36:35 = 5:1]. The mass spectrum of the Knudsen cell effluent during the reaction of N_2O_5 with HCl on wax-coated copper at 185 K (Fig. 3a) shows several new features that indicate heterogeneous reaction on the surface. Increased intensities for mass peaks *m/e* 35 and 37 corresponding to Cl^+ fragments were observed, as well as new mass peaks at *m/e* 49 and 51 corresponding to ClN^+ fragments. The spectrum of $ClNO_2$ ($P = 2$ mtorr) (Fig. 3b), taken under similar conditions, shows the characteristic $ClNO_2$ peaks [*m/e* of 30, 35(37), 46, and 49(51)] along with mass peaks due to a 5% Cl_2 impurity (*m/e* 70, 72, 74). The similarity of Fig. 3, a and b, suggests that the reaction of N_2O_5 with HCl produced $ClNO_2$ in the gas phase. TDS scans after reaction indicated that condensed-phase HNO_3 was formed, as in reaction 4.

The more relevant reaction for the Antarctic stratosphere is the reaction of N_2O_5 on HCl-ice surfaces that simulate PSCs. Solid solutions containing 7% and 14% (per mole basis) HCl in ice were prepared by condensation of gaseous species at 185 K; N_2O_5 reacted rapidly with both surfaces to form gas-phase $ClNO_2$. Mass scans of the Knudsen cell effluent during these reactions were similar to that shown in Fig. 3a. However, the $ClNO_2$ mass peaks were less intense because of lower levels of HCl. No HCl was present in the gas phase over these surfaces ($P < 0.01$ mtorr), and thus no peaks at *m/e* 36 or 38 were observed.

To test the assignment of $ClNO_2$ as a gas-phase product of the reaction of N_2O_5 on HCl-ice, we studied the reaction of $ClNO_2$ on ice at 185 K separately. In contrast to the results for N_2O_5 (Fig. 1), the steady-state $ClNO_2$ ($P = 5$ mtorr) peak intensities did not change upon exposure to ice (Fig. 4). This indicates that $ClNO_2$ does not stick to, or react with, ice at 185 K. This is consistent with the above assignment of $ClNO_2$ as a gas-phase product of the reaction of N_2O_5 with HCl on ice.

We estimated a γ value of 3×10^{-3} for N_2O_5 on HCl-ice after correction of the N_2O_5 mass peak *m/e* 46 for the $ClNO_2$ contribution by assuming a constant *m/e* 46:49 ratio for $ClNO_2$ and assuming that only N_2O_5 and $ClNO_2$ contributed to *m/e* 46. To the extent that other products such as HNO_3 contribute to *m/e* 46, this value must be considered a lower limit.

In order for reaction 4 to be an important source of active chlorine, the HCl within the PSCs must be available for reaction (*16*). Because HCl diffuses readily in ice (*7*), all of the HCl in the bulk ice is expected to be available for reaction with N_2O_5. The HCl content of the ice was measured before and

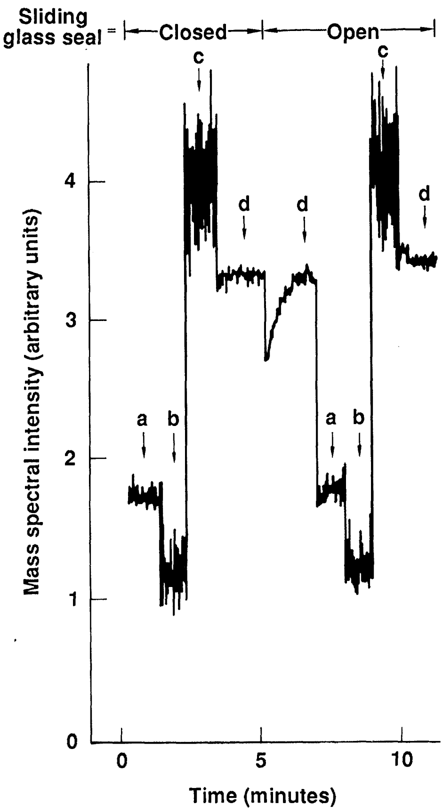

Fig. 4. Mass spectrometer intensities for mass peaks (**a**) *m/e* 30 (expanded $\times$25), (**b**) *m/e* 49 (expanded $\times$2.5), (**c**) *m/e* 35 (expanded $\times$10), and (**d**) *m/e* 46 for the exposure of $ClNO_2$ to ice at 185 K. The ice was exposed to $ClNO_2$ only when the sliding glass seal was in the open position.

after reaction 4. (Reaction 4 was assumed to be complete when the Cl^+ signal was no longer detected.) Although initially the HCl was evenly distributed throughout the ice, the ice remaining after reaction contained less than 5% of the original HCl. This suggests that almost all of the HCl in the ice was available for reaction with N_2O_5.

The mechanism for the reactions of N_2O_5 on ice and HCl-ice surfaces is not known. The rapidity of heterogeneous reactions such as reactions 1 through 4 has led to the suggestion that these reactions are catalyzed by H^+ in the ice (*3, 5*). The facile reaction of N_2O_5 with HCl at low temperatures even in the absence of ice may have mechanistic implications. We cannot rule out possible water impurities below our detection limit (0.01 mtorr) that could influence the reaction mechanism.

Our results indicate that heterogeneous reactions of N_2O_5 with HCl and H_2O occur readily at 185 K, providing a sink for NO_x in the form of condensed-phase HNO_3 and producing photochemically active gas-phase $ClNO_2$. To the extent that the surfaces studied here are similar to PSCs, reactions 3 and 4 may contribute to the photochemical mechanism responsible for ozone depletion in the Antarctic spring.

REFERENCES AND NOTES

1. S. Solomon, R. R. Garcia, F. S. Rowland, D. J. Wuebbles, *Nature* **321**, 755 (1986).
2. O. B. Toon, P. Hamill, R. P. Turco, J. Pinto, *Geophys. Res. Lett.* **13**, 1284 (1986); P. Hamill, O. B. Toon, R. P. Turco, *ibid.*, p. 1288; M. P. McCormick and C. R. Trepte, *ibid.*, p. 1276.
3. P. J. Crutzen and F. Arnold, *Nature* **324**, 651 (1986); P. J. Crutzen, C. Bruhl, U. Schmailzl, F. Arnold, in *Aerosols and Climate*, M. P. McCormick and P. V. Hobbs, Eds. (A. Deepak, Hampton, VA, in press).
4. M. B. McElroy, R. J. Salawitch, S. C. Wofsy, *Geophys. Res. Lett.* **13**, 1296 (1986).
5. S. C. Wofsy, M. J. Molina, R. J. Salawitch, L. E. Fox, M. B. McElroy, *J. Geophys. Res.* **93**, 2442 (1988).
6. J. C. Farman, B. G. Gardiner, J. D. Shanklin, *Nature* **315**, 207 (1985); M. B. McElroy, R. J. Salawitch, S. C. Wofsy, J. A. Logan, *ibid.* **321**, 759 (1986); L. T. Molina and M. J. Molina, *J. Phys. Chem.* **91**, 433 (1987); J. M. Rodriguez, M. K. W. Ko, N. D. Sze, *Geophys. Res. Lett.* **13**, 1292 (1986). For a general review, see R. J. Cicerone, *Science* **237**, 35 (1987).
7. M. J. Molina, T.-L. Tso, L. T. Molina, F. C.-Y. Wang, *Science* **238**, 1253 (1987).
8. M. A. Tolbert, M. J. Rossi, R. Malhotra, D. M. Golden, *ibid.*, p. 1258.
9. M. T. Leu, *Geophys. Res. Lett.* **15**, 17 (1988).
10. H. H. Nelson and H. S. Johnston, *J. Phys. Chem.* **85**, 3891 (1981).
11. These reactions have been reported to occur on laboratory surfaces. See, for example: E. C. Tuazon, R. Atkinson, C. N. Plum, A. M. Winer, J. N. Pitts, Jr., *Geophys. Res. Lett.* **10**, 953 (1983); C. A. Cantrell, J. A. Davidson, R. E. Shetter, B. A. Anderson, J. G. Calvert, *J. Phys. Chem.* **91**, 6017 (1987).
12. W. F. J. Evans, C. T. McElroy, I. E. Galbally, *Geophys. Res. Lett.* **12**, 825 (1985).
13. For a general review of the experimental technique, see D. M. Golden, G. N. Spokes, S. W. Benson, *Angew. Chem. Int. Ed. Engl.* **12**, 534 (1973). The Knudsen cell used in the present experiment consists of two chambers, one of which contains the cold surface of interest. The chambers are separated by a sliding glass seal that can be opened to expose the cold surface to the reactants. The gas-phase contents of the cell were sampled with a mass spectrometer. Reactions on the cold surfaces were monitored by the changes in the mass scans that occurred when the sliding glass seal was opened. Reaction products that remained on the cold surface were detected subsequently by TDS, in which the partial pressures of the products were monitored as the temperature of the surface was increased slowly (3 K per minute). The ice and HCl-ice surfaces were prepared by condensation from the gas-phase onto a halocarbon wax–coated copper block held at 185 K. The N_2O_5 was synthesized as described (*14*). A minor HNO_3 impurity (<1%) was present in the N_2O_5. The $ClNO_2$ used for mass identification and calibration was synthesized as described (*10*).
14. A mass scan at 1.0 mtorr of N_2O_5 revealed no peaks above *m/e* 62 [see L. Brouwer, M. J. Rossi, D. M. Golden, *J. Phys. Chem.* **90**, 4599 (1986)]. A small peak at *m/e* 48, possibly due to ozone impurity, was observed.
15. The sticking coefficient is given by

$$\gamma = (A_h/A_s)\ [(I^0 - I)/I]$$

where A_h and A_s are the areas of the Knudsen cell escape aperture and the surface area of the copper block, respectively, and I^0 and I are the N_2O_5 mass spectrometer signals in the absence and presence of the surface, respectively (*13*).
16. R. R. Friedl, J. H. Goble, S. P. Sander, *Geophys. Res. Lett.* **13**, 1351 (1986).

17. Supported under NSF grant ATM-8600764 and NASA contract NASW-3888.

18 December 1987; accepted 10 March 1988

Evidence for Highly Reflecting Materials on the Surface and Subsurface of Venus

R. F. JURGENS, M. A. SLADE, R. S. SAUNDERS

Radar images at a 12.5-centimeter wavelength made with the Goldstone radar interferometer in 1980 and 1986, together with lunar radar images and recent Venera 15 and 16 data, indicate that material on the surface and subsurface of Venus has a Fresnel reflectivity in excess of 50 percent. Such high reflectivities have been reported on the surface in mountainous regions. Material of high reflectivity may also underlie lower reflectivity surficial materials of the plains regions, where it has been excavated by impact cratering in some areas.

RADAR AND RADIOMETRIC DATA from the Pioneer Venus spacecraft indicate that several regions on Venus have both high Fresnel reflectivity and low radiometric emissivity (*1*). These anomalies are typically associated with mountainous terrain, which has slightly cooler temperatures and increased surface roughness relative to the plains. The lowest emission temperatures reported (about 405 K) were much too low to have been caused by the difference in elevation between the mountains and the plains. Effective dielectric constants that could reduce the emissivity must be large, on the order of 30. Such high values are larger than those expected for basalt and most other nonigneous rocks. Pyrite inclusions in the rocks have been suggested as a mechanism to increase the conductivity of the material sufficiently to increase the reflectivity and reduce the emissivity (*1*).

We provide radar evidence that material with high Fresnel reflectivity also occurs in the low plains regions where the temperature is near 735 K. We examined radar images that were made with the Goldstone triple interferometer during the inferior conjunctions of 1980 and 1986. The observations were made at a wavelength of 12.5 cm with circularly polarized waves. Right-circular polarization was transmitted, and left-circular polarization was received; this method captures the waves scattered by the quasi-specular scattering mechanism. We concentrated on images from regions within 5° to 7° of the subradar point because these images have the highest possible signal-to-noise ratio. The data acquisition and data processing procedures are given in (*2*), except that high-resolution, digital-acquisition equipment was used during the 1986 observations. This equipment substantially improved the best linear resolution of our images from about 8 km to about 1.3 km without serious loss of coverage.

Several of our reduced radar images show bright features that extend through a range of incidence angles of several degrees. The contrast of these features relative to their environs remains nearly constant with angle. These bright features are most easily explained by large values of the Fresnel reflection coefficient on the surface. The most striking is a large bright feature in the northern hemisphere that extends over an angular range from roughly 3° to 7° (Fig. 1A). The radar albedo locally is nearly four times as great as the average surface albedo (*3*). Although the companion altimetry image (Fig. 1B) for the region suffers from

---

Jet Propulsion Laboratory, California Institute of Technology, 4800 Oak Grove Drive, Pasadena, CA 91109.